Physical Properties of Interfacial Layers Developed on Weathered Silicates: A Case Study Based on Labradorite Feldspar

Bastien Wild, Damien Daval, Jean-Sébastien Micha, Ian Bourg, Claire E White, Alejandro Fernandez-Martinez

To cite this version:

Bastien Wild, Damien Daval, Jean-Sébastien Micha, Ian Bourg, Claire E White, et al.. Physical Properties of Interfacial Layers Developed on Weathered Silicates: A Case Study Based on Labradorite Feldspar. Journal of Physical Chemistry C, 2019, 123 (40), pp.24520-24532. 10.1021/acs.jpcc.9b05491 . hal-02372378

HAL Id: hal-02372378
https://hal.science/hal-02372378v1

Submitted on 20 Nov 2019

Physical Properties of Interfacial Layers Developed on Weathered Silicates: a Case Study Based on Labradorite Feldspar

Bastien Wild[1,2,3,*], *Damien Daval*[1], *Jean-Sébastien Micha*[4], *Ian C. Bourg*[3,5], *Claire E. White*[2,3] *and Alejandro Fernandez-Martinez*[6]

AUTHOR ADDRESS

[1] Laboratoire d'Hydrologie et de Géochimie de Strasbourg (LHyGeS), Université de Strasbourg /EOST-CNRS UMR 7517, 1 Rue Blessig, 67000 Strasbourg, France

[2] Andlinger Center for Energy and the Environment, Princeton University, Princeton, NJ 08544, USA

[3] Department of Civil and Environmental Engineering, Princeton University, Princeton, NJ 08544, USA

[4] CEA - Grenoble/INAC/SPrAM, 17 rue des Martyrs, 38041, Grenoble, France

[5] Princeton Environmental Institute, Princeton University, Princeton, NJ 08544, USA

[6] Univ. Grenoble Alpes, Univ. Savoie Mont Blanc, CNRS, IRD, IFSTTAR, ISTerre, Grenoble 38000, France

*Corresponding Author : bwild@princeton.edu ; (609) 986 6332

ABSTRACT

Amorphous silica-rich surface layers (ASSLs) formed at the interface between silicate materials and reacting fluids are known to strongly influence, at least in some cases, the dissolution rates of silicate phases including soil minerals, glasses, and cements. However, the factors governing the formation of these ASSLs remain largely unknown. Here, we outline a novel approach that uses recent developments in vertical scanning interferometry (VSI) and in-situ synchrotron-based X-ray reflectivity (XRR) to directly follow the development of ASSLs, and the evolution of their physical properties, on a model silicate (labradorite feldspar). Our approach enabled independently probing the reactivities of the outer (bulk fluid/ASSL) interface and of the inner (ASSL/pristine mineral) interface *in-situ*, providing a detailed picture of the temporal evolution of the fluid-mineral interface. We investigated the effects of pH, SiO_2(aq) concentration, crystallographic orientation, and temperature on the layer thickness, density, and reactivity as well as on the dissolution rate of the primary mineral. The dissolution rate of labradorite crystals increased with temperature, according to an apparent activation energy of ~57 kJ mol^{-1} and showed no significant difference between crystallographic faces. Both labradorite and ASSL dissolution rates decreased as circum-neutral pH conditions were approached. High SiO_2(aq) concentrations resulted in (i) decreased apparent dissolution rates, while far-from-equilibrium conditions with respect to labradorite were maintained in the bulk fluid, and (ii) an increasing ASSL density when combined with low temperature and close-to-neutral pH. Our results highlight the importance of ASSLs and their complex impact on the dissolution process. In particular, our results provide evidence of a discrepancy between bulk fluid conditions, generally probed and reported, and those actually operating at the interface with the dissolving primary

phase, which are of more direct relevance to the dissolution process but are still largely unknown.

INTRODUCTION

Amorphous silica-rich surface layers (ASSLs) are hydrated, nanoporous, metastable phases that form at the interface between reactive fluids and a variety of silicate materials including olivine [1-4], wollastonite [5-9], feldspars [10-14], and glasses [15-18]. These layers, also called surface alteration layer (SAL), form ubiquitously from laboratory to field settings [19-21]. They play a key role in controlling the dissolution rates of silicate materials with important implications for several critical environmental and societal challenges including the degradation of cement infrastructure [22], the long-term storage security of nuclear waste [18,23], and the feasibility of enhancing silicate weathering as a large-scale CO_2 capture technology [24,25].

While the existence of ASSLs has been known or hypothesized for at least 80 years [26], the mechanisms underlying their formation and their influence on the dissolution rate of the primary material remain poorly understood. This lack of mechanistic understanding is illustrated by two fundamental disagreements. The first of these concerns whether ASSLs form by leaching of soluble elements (e.g., Ca, K, Mg, Na) from the primary mineral or, alternatively, by dissolution of the primary mineral followed by precipitation of an amorphous Si-rich phase. The first hypothesis (referred to as the “leached layer” hypothesis) has represented the prevailing paradigm for decades [27,28]. It is consistent with ion and photon probe results suggesting that the elemental profiles of reactive species and reaction products are anticorrelated within the ASSL [29-38]. The alternative “dissolution-reprecipitation” hypothesis [39] is supported by transmission electron microscopy observations that indicate an absence of compositional gradients within the ASSL [13] and atom-probe tomography measurements of altered glass samples that reveal an atomically sharp inner interface {Gin, 2017; Hellmann, 2015}, which has led to the suggestion that the compositional gradients observed in the ion and photon probe results may be artifacts associated with low lateral resolution [20]. It is also supported by indirect evidence, in some cases, of fluid-mineral interactions occurring through the layer and of mineral dissolution at the interface between the ASSL and the pristine mineral surface [40], due to the presence of a thin fluid film at the inner interface {Hellmann, 2012}.

The second fundamental disagreement concerns the extent to which the ASSL behaves as a barrier to transport. The historical approach assumes that the dissolution rate of the pristine silicate mineral surface follows transition state theory (TST) and depends only on the chemistry of the bulk aqueous solution [41]. This “primary dissolution control” approach was based on studies where the presence of ASSLs had little or no effect on the dissolution rate or where evidence of diffusive processes was dismissed as experimental artefacts [10,42-44]. While challenged more than 20 years ago by both contradictory experimental results [45,46] and theoretical inconsistencies [47,48], this hypothesis is still widely used in reactive transport codes. An important alternative (referred to as the “ASSL dissolution control” approach) consists in applying TST while treating the thermodynamic properties of the ASSL (rather than the primary mineral) as a driver of the overall weathering process [45,49-53]. In essence, this approach treats the ASSL as an activated complex in the sense of TST, the experimental verification of which is still a subject of debate [54]. A second important alternative (referred to as “primary dissolution and transport control”) suggests that, in addition to the dissolution of the primary mineral, transport limitations to the diffusion of reactive species across the ASSL must also be accounted for [9,18,55-59].

One reason for the existence of competing modeling frameworks outlined above is the relatively limited availability of dissolution data relative to the vast range of conditions to be explored in terms of silicate mineral chemistry, aqueous chemistry, and temperature. For example, with the notable exception of results obtained on wollastonite over a wide pH range [20], most studies supporting the hypothesis that chemical affinity between the bulk fluid and the primary mineral plays an important role were performed under low pH conditions, which favor the formation of non-passivating layers [14], similar to the work by Lagache [10] more than 40 years ago. Similarly, parameters such as the redox potential of the solution that have not been systematically examined may have a direct impact on ASSL texture and resulting diffusivity [60-62]. In short, competing interpretations regarding the mechanism and impact of ASSL formation on the overall silicate dissolution rate for identical materials (e.g., Schott, et al. [8] vs. Ruiz-Agudo, et al. [7] or Hellmann, et al. [63] vs. Gin, et al. [18]) may simply reflect differences in reacting conditions combined with insufficient knowledge of the thermodynamic and transport properties of ASSLs.

The upshot of this is that an improved understanding of the fundamental properties of ASSLs is likely key to resolving the disagreements outlined above [25,64]. Existing data on the properties of ASSLs remains relatively limited for several reasons. First, standard dissolution experiments yield relatively low accuracy estimates of the growth rate of the ASSL as quantified indirectly from small deviations between the stoichiometric composition of released elements and that of the pristine solid. Second, reconstructions of mineral dissolution rates and ASSL thickness from elemental release data are challenged by uncertainties related to the specific surface area of the reactive interface, typically estimated as the Brunauer-Emmett-Teller (BET) surface area of the fresh mineral powder [65]. Such normalization may not account for the temporal evolution of reactive surface area or spatial variability of the dissolution rate, while the surface area measurement itself may be inconsistent and carry large and often poorly constrained uncertainties [66]. Finally, the few existing detailed characterizations of ASSLs have been carried using destructive techniques and, therefore, they inherently do not reveal the time-dependence of ASSL properties.

To date, the transport properties of nanoporous surface layers developed on silicate materials have represented a recurrent topic for material scientists in general and have been addressed by theoretical and experimental studies beyond the field of Geosciences [57,67-71]. Importantly, such transport properties are critically inherited from the (yet to be determined) physicochemical evolution of the silica-rich surface layers, which represent some of the central insights to this study.

The aim of the present study is to utilize a novel combination of approaches to follow the evolution of the physical properties of ASSLs *in-situ*, providing direct information into ASSL thickness and density and indirect insights into the local physico-chemical conditions prevailing at the inner (pristine mineral/ASSL) interface. We use X-ray reflectivity (XRR) data to track the temporal evolution of ASSL thickness and density. Complementary vertical scanning interferometry (VSI) measurements are performed to track the evolution of the outer (ASSL/bulk solution) interface. Our methodology circumvents the aforementioned challenges and enables probing mineral reactivity and layer formation at low solid/fluid ratios (~21 mm^2 for 800 ml of solution), ensuring that far-from-equilibrium conditions with respect to the dissolving crystal can be maintained. Layer thickness and surface retreat data are combined to determine the rate of retreat of the inner interface, enabling the calculation of the dissolution rate of the primary labradorite feldspar located underneath the ASSLs. Overall, this study provides a novel characterization of the physicochemical properties of nanoporous surface layers developed on a reference silicate material (feldspar), with possible consequences for the dissolution kinetics of the underlying substrate.

METHODS

Sample preparation

Labradorite single crystals from Nuevo Casas Grande, Chihuahua (Mexico) were provided by the Mineralogical & Geological Museum of Harvard University (Ref. MGMH#135998). They consist of transparent gem-grade crystals with a composition of $Ab_{39}An_{60}Or_1$ [72]. Samples of about 7 mm × 3 mm suited for XRR, VSI, and atomic force microscopy (AFM) measurements were prepared following standard procedures previously described [14]. Briefly, euhedral crystals were cut with a diamond saw following (001) preferential cleavage planes and polished down to the nanometer scale using colloidal silica polishing suspension. One (010) surface was also prepared. Their orientation was verified by indexing electron backscatter diffraction (EBSD) patterns obtained on a Tescan Vega 2 scanning electron microscope (SEM).

Labradorite dissolution and ASSL formation

Labradorite samples were reacted in pH environments ranging from 1.5 to 4 and experiments were run for durations of about 1 hour to more than 35 days as required to form measurable (i.e., > 5 nm thick) ASSLs at the fluid-mineral interface. Samples were incubated at 80°C using (PTFE) Savillex® reactors equipped with a custom PTFE stirring system [14]. Reactors were filled with a reacting fluid consisting of Milli-Q water whose pH had been previously adjusted with high-grade HCl (37%, ACS reagent) and, for some experiments, saturated with respect to amorphous silica using sodium metasilicate, nonahydrate (Sigma Aldrich®, >98%).

The pH was regularly controlled and adjusted if necessary. A summary of experiments and experimental conditions can be found in Tables S1-S6. The saturation indices for labradorite and amorphous silica at 80 °C were calculated using the Chess® software and the Chess® tdb database. After reaction, samples were briefly rinsed in Milli-Q water and kept at room temperature in aqueous solutions close to saturation with respect to amorphous silica until XRR measurement to avoid subsequent dehydration or dissolution. For experiments carried out over short durations (up to 94 hours), crystals were directly reacted *in-situ* over the course of the XRR measurements with an experimental setup enabling fluid circulation at controlled temperature in a custom flow-through cell with Kapton windows (Figure 1).

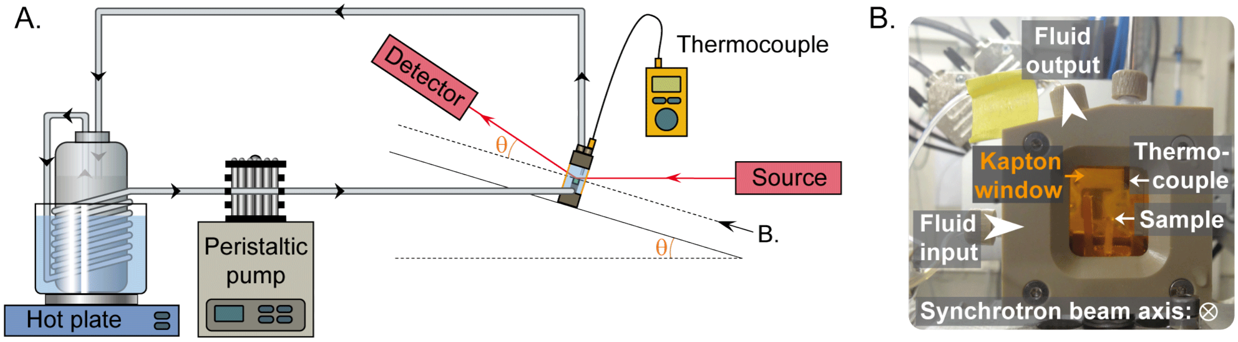

Figure 1. overview of the experimental setup (A) and front view of the flow-through cell designed for *in-situ* experiments (B). Fluid temperature within the cell was verified with a thermocouple.

Dissolution rate at the outer interface by vertical scanning interferometry

The topography of each labradorite sample was measured on a Zygo New View 7300 VSI prior to reaction. A portion of the surface of samples summarized in Tables S5 and S6 was then masked with a room-temperature-vulcanizing (RTV) silicone glue spot in order to create a non-reacted reference by avoiding fluid-mineral contact at this specific location. After reaction, the global retreat of the surface due to crystal dissolution was quantified using topography images recorded by VSI on reacted samples after removal of the mask. The absolute dissolution rate at the fluid/layer interface is estimated as $r = (\Delta h/\Delta t) \times (1/V_\mathrm{m})$, where r stands for the absolute dissolution rate (mol $\mathrm{m^{-2}\ s^{-1}}$), Δh is the surface retreat (m), Δt is the alteration duration (s), and V_m is the molar volume of labradorite ($\mathrm{m^3\ mol^{-1}}$) [73]. Topography images and profiles were analyzed using SPIP software.

The roughness of the outer interface, σ_{ex}, was determined based on AFM (Bruker Multimode AFM) and VSI measurements conducted on three representative portions of the surface with dimensions of 1 µm × 1 µm (AFM) and 125 µm × 125 µm (VSI). The roughness value was calculated using Gwyddion software [74] as the root mean square of the deviations in height z from the mean image data plane z_0. Nanoscope Analysis software and Gwyddion were used to visualize and process AFM data including particle size measurements.

Internal properties of the ASSL by *in-situ* X-ray reflectivity experiments

X-ray reflectivity measurements were performed at the European Synchrotron Radiation Facility (ESRF) at the French BM32 beamline (CRG-IF). 27 keV X-rays (wavelength, λ = 0.0459 nm) were used to ensure sufficient transmission (T ~ 68.5%) through the ~1 cm thick solution in the cell. Reflectivity patterns were acquired for 2θ angles ranging between 0° and 1° (corresponding to scattering vectors ranging between 0.0 and 0.5$\mathrm{Å^{-1}}$). For the pre-reacted samples (i.e., samples reacted prior to the XRR measurement campaign), the dissolution experiments had different onset times and were all stopped one day prior to the XRR campaign, yielding samples altered for a range of desired time periods. The pre-reacted samples were then transported to the ESRF in a near-neutral pH solution (pH~6.5) saturated with respect to amorphous silica. Once at the ESRF, pre-reacted samples were analyzed in our custom cell

(Figure 1B) filled with Milli-Q water at room temperature. For the *in-situ* experiments, unreacted samples were placed in the same cells circulated with fluid of desired chemistry at 80°C and patterns were acquired every 5 to 15 min depending on the growth rate of the ASSL (Figure 1).

Reflectivity data were fitted using the analysis package Motofit [75], which runs under the IGOR Pro environment. Interfacial roughness, layer density (initially set to that of pure amorphous silica), and layer thickness were refined to match the scattering length density (SLD) profile q(*z*) in the direction perpendicular to the mineral-water interface. The strategy used to fit the experimental XRR patterns involved the minimum number of layers required to obtain a satisfactory fit following Nelson [75] . Discrepancies between the model and data were quantified by the χ^2 parameter as defined by Nelson [75] , which was minimized by adjusting the thickness and SLD parameters of each layer as well as inner and outer roughness values following a two-step procedure including genetic optimization [76] and the Levenberg-Marquardt method [77]. As shown in Figure S1, some factors (for example, the existence of local minima) were found to have non-monotonic influence on fit quality as quantified by the χ^2 value. Hence, the reliability of data modeling was ensured by including genetic optimization as the first step of the fitting procedure. All possible solutions were analyzed manually and discarded if necessary (for instance in the case non-realistically high density values).

RESULTS

Formation of ASSLs and *in-situ* evolution of their physical properties

The formation of ASSLs at the fluid-mineral interface was observed by XRR for all tested conditions, i.e. pH = 1.5 to pH = 4, 80°C or 25°C, in aqueous solutions that were either saturated or not with respect to amorphous silica. As a general trend, ASSLs' growth rate decreases for experiments conducted at higher pH values, in solutions saturated with respect to amorphous silica or at lower temperature, all other conditions being kept constant. The ASSL was found to grow at a nearly constant rate in most conditions as revealed by the linear trends in Figure 2, with the notable exception of the longest experiments conducted at pH = 3 and 4 (duration ≥ 1 day). Comparison between results at different pH values revealed a near-linear pH-dependence of the logarithm of the growth rate (Figure 3). Use of a lower temperature (25 vs. 80°C at pH = 1.5) in saturated solution led to a drop of the dissolution rate by a factor of ~50 (orange symbol, Figure 3). Fluid saturation with respect to amorphous silica led to a decrease of the growth rate by a factor ranging from ~4 at pH = 1.5 to nearly 30 at pH = 4 (diamonds versus squares, Figure 3).

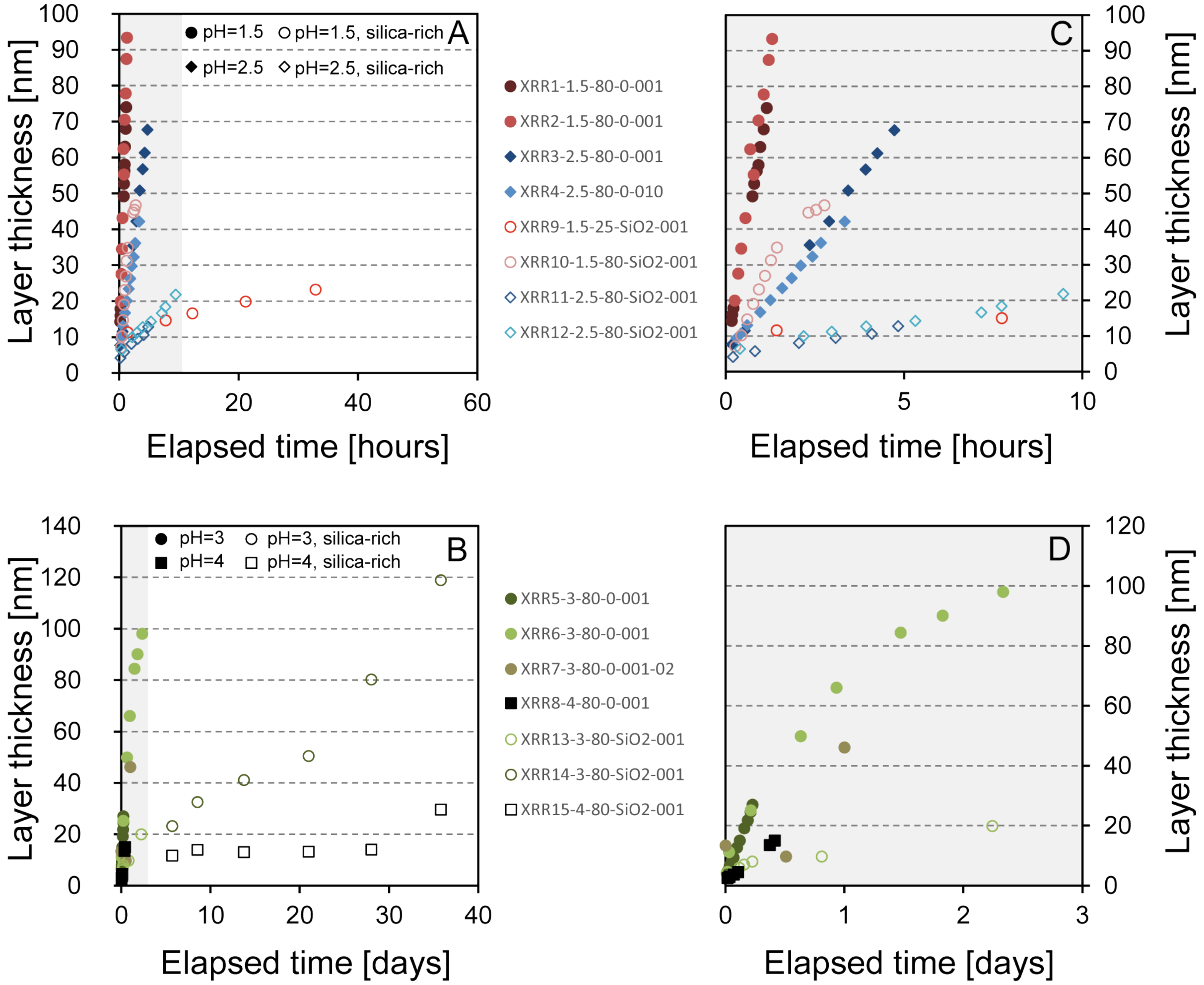

Figure 2. Temporal evolution of layer thickness as measured by X-ray reflectivity. Layers' growth was generally faster for experiments at pH ≤ 2.5 (A) compared to experiments at pH > 2.5 (B), and slower for experiments conducted with fluids saturated with respect to amorphous silica (open data points) compared to their non-saturated counterparts (filled data points). All experiments were conducted at 80°C with the exception of experiment XRR10-1.5-25-SiO2-001 (red open circles in panel A), conducted at 25°C.

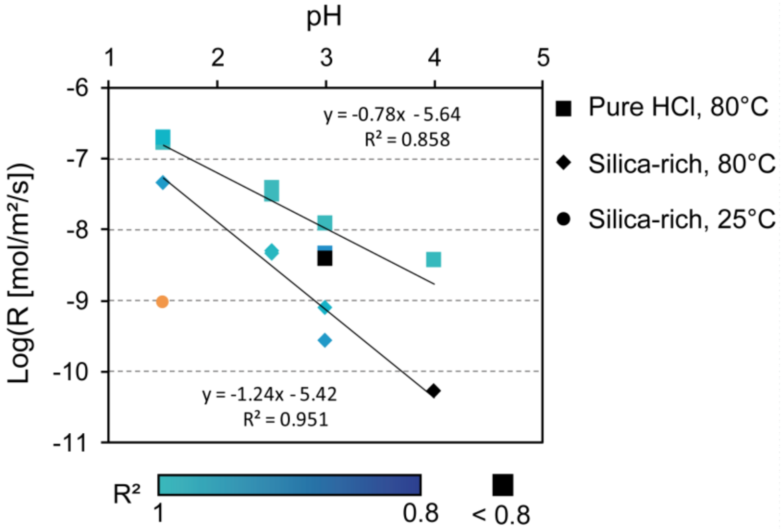

Figure 3. pH-dependence at 80°C of layer growth rate represented as moles of labradorite per square meter converted each second into layer ($labradorite \rightarrow layer$). Diamonds and squares represent experiments where the fluid was saturated or not with respect to amorphous silica, respectively. For each experiment represented here, the color quantifies the regression coefficient associated to linear regression of the temporal evolution of the layer thickness (cf. Figure 2) according to the color scale below the graph. The orange data point corresponds to the experiment conducted at 25°C in a silica-rich fluid.

Measured SLD values ranged from 10.6 to 21.5 10^{-6} Å^{-1}, which would correspond to densities of ~1.25 and 2.53 g cm^{-3} under the hypothesis that ASSL are composed of pure silica (SiO_2) (Figure 4). No significant SLD difference (within the uncertainty of ± 5 %) was detected between ASSLs grown on different crystallographic surfaces [(001) vs. (010)]. Experiments conducted in fluids combining high Si concentrations (~145 ppm) and weakly acidic pH or low temperature (e.g. experiments XRR10-1.5-25-SiO2, XRR14-3-80-SiO2-001 or XRR15-4-80-SiO2-001) tended to exhibit constant or increasing SLD trends over time, suggesting progressive densification. Conversely, experiments conducted in fluids with low Si concentrations (< 200 ppb) exhibited decreasing, constant, or non-monotonous SLD trends. The experiment conducted at 25°C in a silica-rich fluid at pH=1.5 exhibited a significantly lower mean SLD compared to its counterpart conducted at 80°C (12.8 ± 0.9 vs. 14.8 ± 0.5 respectively). Measurements performed after completion of experiments XRR9-1.5-80-SiO2-001, XRR11-2.5-80-SiO2-001 and XRR13-3-80-SiO2-001 revealed that layers dried and measured immediately after *in-situ* dissolution tend to exhibit lower SLD values than previous measurements corresponding to their hydrated counterparts (Table S3).

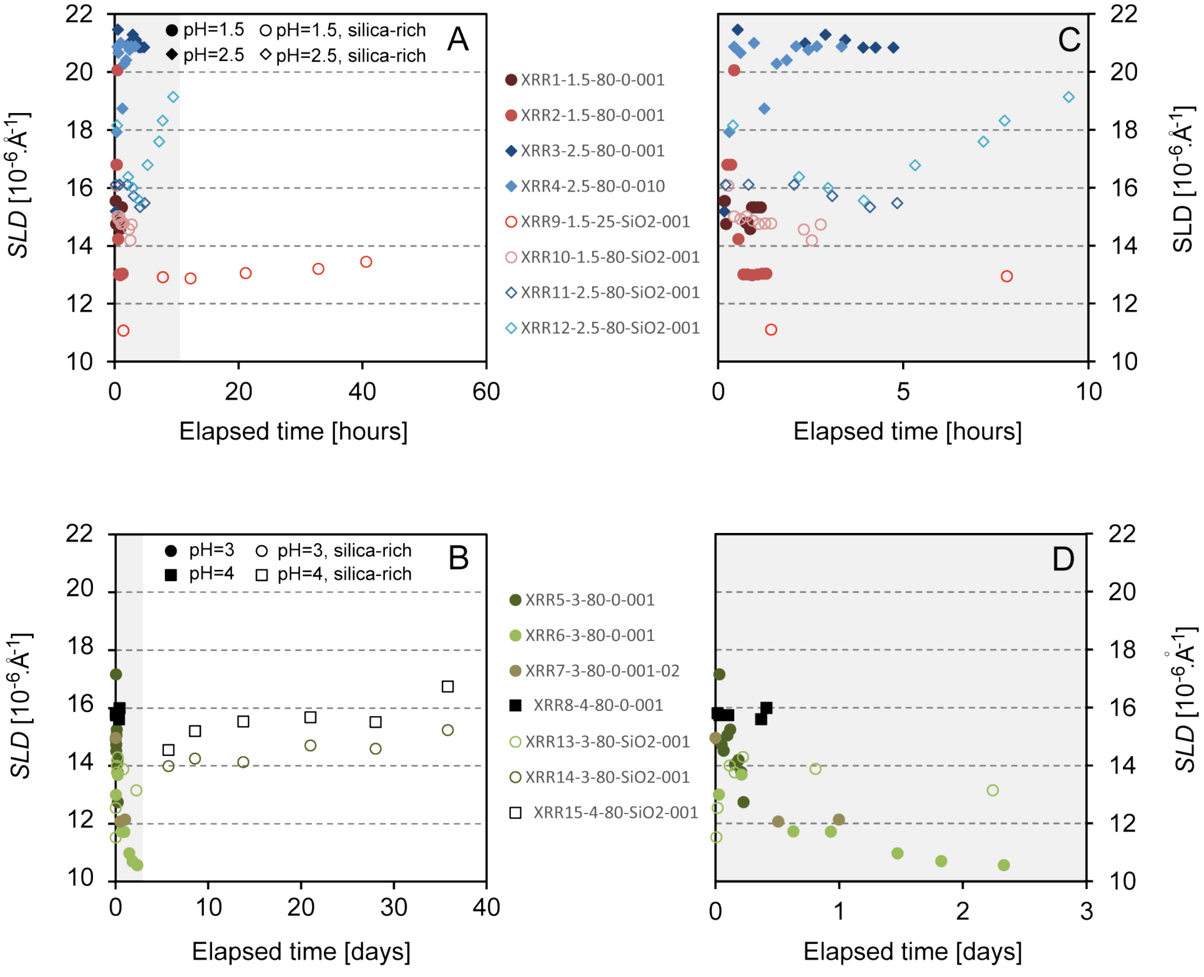

Figure 4. Temporal evolution of the scattering length density of ASSLs as measured by X-ray reflectivity for experiments at pH ≤ 2.5 (A, C) and pH > 2.5 (B, D). Open data points correspond

to experiments conducted with fluids saturated with respect to amorphous silica. C and D correspond to close-up views of the regions indicated by the shaded areas on plots A and B, respectively. All experiments were conducted at 80°C with the exception of experiment XRR10-1.5-25-SiO2-001 (red open circles in panel A), conducted at 25°C.

Reactivity and evolution of the outer interface

The global retreat of the outer surface compared to a masked reference (Figure 5), as measured using VSI, was used to probe the reactivity at the outer (ASSL/bulk solution) interface in all tested conditions (see Tables S5 and S6) on a set of samples distinct from those dedicated to XRR measurements.

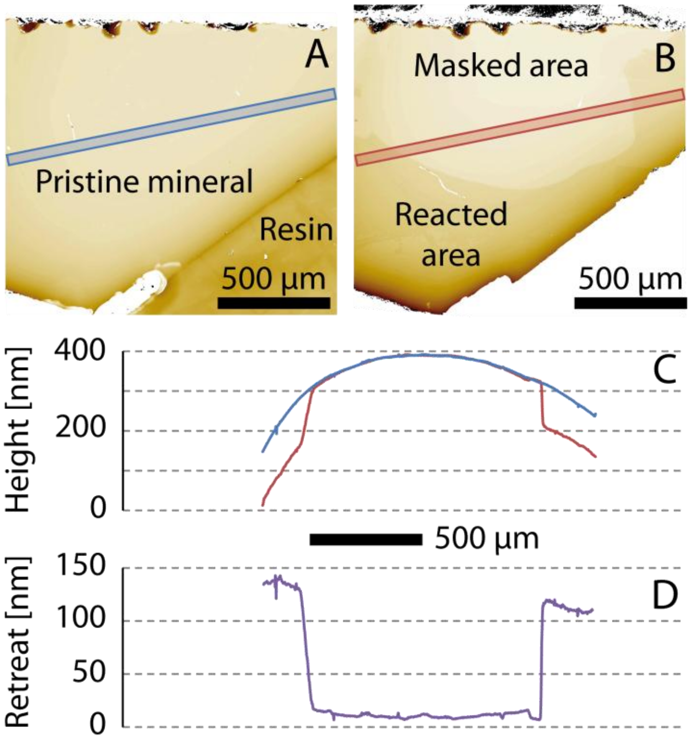

Figure 5. Typical measurement of surface retreat based on topography maps acquired by VSI before (a) and after (b) the dissolution process (here a labradorite sample weathered for 35 days

at 80°C in a fluid at pH = 3 saturated with respect to amorphous silica). This specific sample was detached from the resin after reaction to facilitate VSI alignment. Height profiles recorded before (blue) and after (red) weathering through the non-reacted masked area are superimposed (c) and subtracted to highlight the overall surface retreat. Some variation on the retreat can be seen, which is consistent with literature on intrinsic variability of the dissolution rate and profile subtraction at the mm scale.

Assuming isovolumetric weathering, dissolution rates of the outer interface were reconstructed from VSI data and showed a significant decrease with increasing pH (Figure 6). Dissolution rates were smaller when the bulk fluid was saturated with respect to amorphous silica, indicating a decreased reactivity of the ASSL at the outer interface by a factor of 4 to 80. The high vertical resolution of the VSI measurements (down to a few nm) enabled estimating the apparent activation energy (E_a) of the ASSL dissolution process based on kinetic data collected at T_1 = 80°C and T_2 = 25°C for experiments with a fluid at pH = 1.5 saturated with respect to amorphous silica, as:

$$E_a = R\frac{T_1 T_2}{T_1 - T_2}\ln\left(\frac{r_1}{r_2}\right) \tag{1}$$

where r is the dissolution rate of ASSL. In these conditions, the ~23-fold decrease in ASSL dissolution rate between 80°C and 25°C corresponds to an E_a value of 50 kJ mol^{-1}.

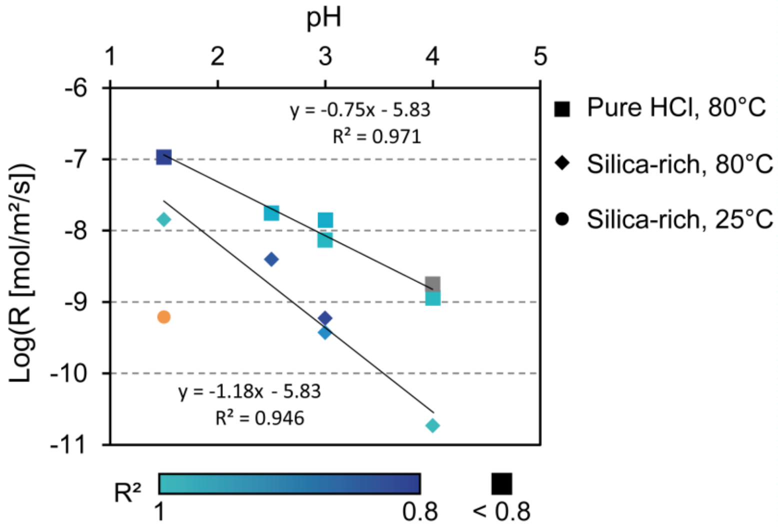

Figure 6. pH-dependence of layer dissolution rate (*layer→dissolved species*) at 80°C. Diamonds and squares represent experiments where the fluid was saturated or not with respect to amorphous silica, respectively. For each experiment represented here, the color quantifies the regression coefficient associated to linear regression of the temporal retreat of the outer fluid/layer interface (cf. Figure 7) according to the color scale below the graph. Grey square: based on 2 retreat values. The orange data point corresponds to the experiment conducted at 25°C in a silica-rich fluid.

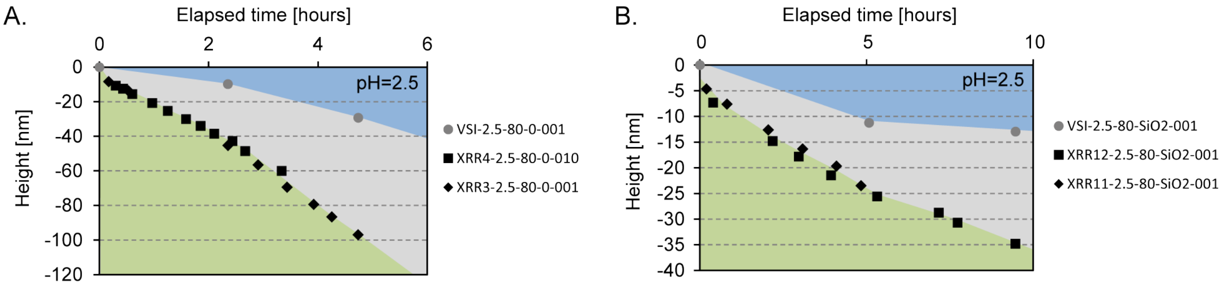

Figure 7. Temporal evolution of ASSL thickness (grey) at the interface between mineral (green) and fluid (blue) for experiments conducted at 80°C, pH=2.5), using a fluid that was saturated (SiO_2, panel B) or not (0, panel A) with respect to amorphous silica. Grey dots correspond to VSI

measurements of the surface retreat compared to a non-reacted reference (zero height) and track the reactivity of the outer interface. Black diamonds and squares correspond to X-ray reflectivity data corrected for surface retreat and track the temporal evolution of the inner interface. Colored background is used to guide the eye. All experiments were conducted on (001) labradorite faces with the exception of one experiment conducted on (010) (A). A summary of all experimental conditions tested in this study can be found in Figure S3.

The roughness of the outer interface of a sample reacted at pH=3 was measured before and after dissolution on AFM and VSI data [14,78]. Both techniques yield roughness values of similar order of magnitude, the VSI measurements being nevertheless systematically higher than those from AFM. During the experiments, roughness increased from σ_{ex}^{VSI}= 17 nm and σ_{ex}^{AFM}= 7 nm to σ_{ex}^{VSI}= 65 nm and σ_{ex}^{AFM}=36 nm as measured using VSI and AFM, respectively. AFM measurements further showed the formation of a nanoscale botryoidal texture of the outer interface exhibiting spherical particles with an average radius of 9.8 ± 1.2 nm (Figure S2). In order to estimate a maximal porosity formed by the silica beads constituting the layer (as opposed to a dense packing of these particles), their arrangement at the outer interface was studied based on AFM data. The intersection of particles with a plane located 9.8 nm below the highest point of a representative portion of the fluid/layer interface yields a pore/particle ratio of 3.2, which yields a rough estimate of ~0.76 as an upper bound on the porosity of the ASSL.

Temporal evolution of the fluid-silicate interface and labradorite reactivity

VSI and XRR data were combined to provide one of the first accurate representations of the temporal evolution of the fluid-silicate interface during dissolution and layer formation (Figure 7, Figure S3). In particular, the surface retreat z_{out} measured by VSI was combined with the ASSL thickness Δz determined from XRR data to evaluate the absolute height of the inner interface z_{in} (black squares and diamonds, Figure 7) at each timestep t:

$$z_{in}(t) = -\Delta z(t) - \frac{z_{out}(t_{+1}) - z_{out}(t_{-1})}{t_{+1} - t_{-1}} * t \tag{2}$$

In equation 2, $\Delta z(t)$ is evaluated at time t by XRR, while $z_{out}(t_{+1})$ and $z_{out}(t_{-1})$ correspond to absolute values of the surface retreat at the closest VSI measurement before and after XRR measurement respectively. In most cases, the temporal evolution of the inner interface was linear or made up of linear portions of curves, which indicates constant dissolution rate at given experimental conditions. Linear regression of z_{in} vs. time was used as a proxy to estimate the overall reactivity of labradorite (i.e., the dissolution rate of the primary mineral). Of note, this approach considers the ASSL/mineral boundary as a single interface since the two reaction fronts located on each side of the thin fluid film often reported at the inner interface {Hellmann, 2012}, could not be resolved by XRR. The resulting retreat rates of the inner interface revealed a near logarithmic dependence of the dissolution rate on pH (Figure 8). Saturation of the solution with respect to amorphous silica decreased the dissolution rate by a factor ranging from ~5 at pH = 1.5 to ~50 at pH = 4. A temperature decrease from 80°C to 25°C at pH = 1.5 yielded a 37-fold drop in dissolution rate corresponding to an apparent energy of activation of about 57 kJ mol^{-1}.

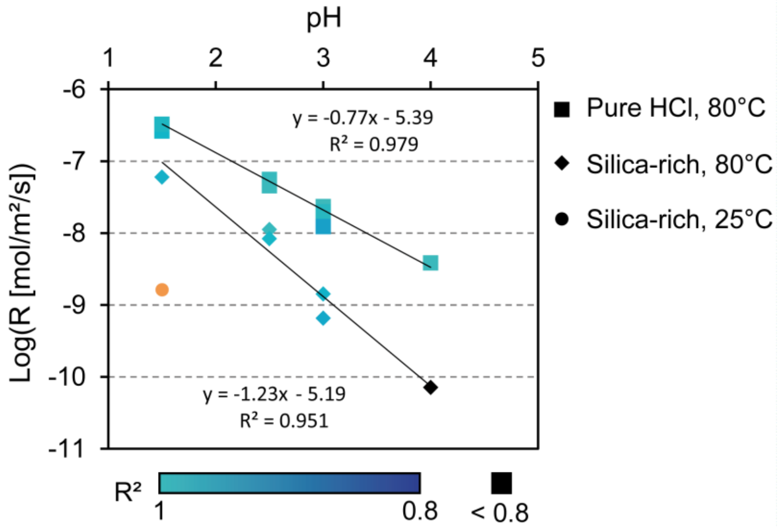

Figure 8. pH-dependence at 80°C of labradorite dissolution rate ($labradorite \rightarrow layer + dissolved\ species$). Diamonds and squares represent experiments where the fluid was respectively saturated or not with respect to amorphous silica. For each experiment represented here, the color quantifies the regression coefficient associated to linear regressions of the temporal retreat of the inner layer/mineral interface (cf. Figure 7) according to the color scale below the graph. The orange data point corresponds to the experiment conducted at 25°C in a silica-rich fluid.

Fluid saturation state

To verify that all our experiments were conducted at far-from-equilibrium conditions with respect to labradorite dissolution (*i.e.*, in the region where the dissolution rate is invariant with saturation state, which defines the dissolution rate plateau), we used the final surface retreat and layer thickness, along with the known sample geometric surface area ($\sim 2.8\times10^{-5}$ m^2) and labradorite density ($\sim 9.8\times10^{-5}$ m^3 mol^{-1}), to estimate the maximum possible fluid saturation state with respect to labradorite at the end of our experiments. We note that rough samples edges resulting from diamond saw cutting were washed and covered with RTV glue prior to experiment, which limited their contribution to cation release to the solution composition. As shown in Table S1, Gibbs free energy (ΔG_r) values were all below the ΔG_r threshold value of -41.8 kJ mol^{-1} where labradorite dissolution should be invariant with saturation as reported by Taylor, et al. [46].

DISCUSSION

Fitting X-ray reflectivity data

During the XRR fitting procedure, four parameters describing the ASSL were adjusted to match the reflectivity data. These parameters include the layer thickness, density, as well as its inner and outer roughness. Since the thickness of the layer primarily affects the periodicity of the signal, which is not significantly impacted by density or roughness, this parameter can be independently assessed with a high degree of confidence. The three other parameters are somewhat correlated, so that the choice of a "best fit" solely based on the χ^2 minimization criterion is non-trivial (see e.g. Figure S1) and sometimes implicitly corresponds to favoring the fitting of one portion of the curve relative to another. Indeed, since the χ^2 value depends on the proportion of data points accurately fitted by the model, it is possible to get a lower χ^2 value with a less relevant fit if parts of the curve containing little information (as opposed to "features of interest" such as critical angle or well-defined oscillation region), account for a large proportion of the considered data points.

In an attempt to alleviate the issue identified above, we constrained our estimate of the roughness of the outer interface using roughness values measured on the same sample before and after dissolution. We note that these independent roughness measurements had to be performed *ex-situ*, which prevented the acquisition of a time-series during the experiment. We associated as a first approximation σ_{ex}^{XRR} either to the linear interpolation of initial and final AFM-based roughness (σ_{ex}^{AFM}, cf. dark grey squares, Figure 9) or to the interpolation of the initial and final averages between VSI- (σ_{ex}^{VSI}) and AFM- (σ_{ex}^{AFM}) based roughness (cf. light grey squares, Figure 9). Reflectivity measurements performed on dried layers (Table S3) were used to verify that any observed discrepancy between σ_{ex}^{XRR} and σ_{ex}^{VSI} or σ_{ex}^{AFM} was unlikely due to dehydration of ASSLs. After applying this constraint, the best fit to the XRR data for both methods (referred to as "AFM/VSI roughness fit" and "AFM roughness fit" and shown as light and dark grey squares in Figure 9B) based on the two remaining parameters (ASSL density and the roughness of the inner interface) suggested that the density of the ASSL invariably increases with time, in contrast with the conclusions reached from the analysis solely based on the χ^2 minimization criterion. However, the resulting density values exceeded those of pure amorphous silica (~20.6 $\times 10^{-6}.A^{-2}$) and even those of unreacted labradorite ($23.5\times 10^{-6}.A^{-2}$). This likely unphysical result suggests that the roughness values derived by both AFM and VSI overestimate the roughness reflected by the XRR results. Consequently, we decided to rely on the well-documented "χ^2 fit" approach [75], which also enables direct comparison of our data with literature [9,56]. We note however that surface roughness may artificially lower the layer apparent density and that further research should be directed at better characterizing the *in-situ* evolution of surface roughness with relevant experimental probes.

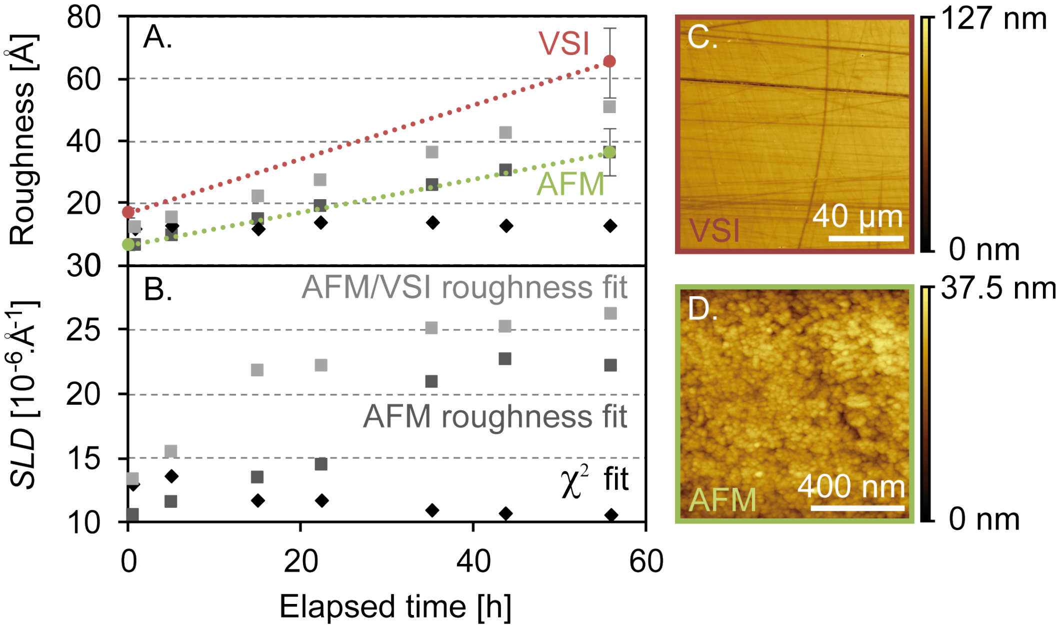

Figure 9. Temporal evolution of roughness (A) and SLD (B) for experiment XRR6-3-80-0-001. Black diamonds correspond to the best fits determined using the lowest χ2 value as the criterion to assess the validity of the fit, grey squares correspond to best fits obtained using the lowest χ2 value after imposing at each temporal step the roughness at the outer interface based on topography measurements. In that case, the roughness at the inner interface and the density of the layer were the only adjustable parameters of the model (see text for details). For the “AFM roughness fit” (dark grey squares), the evolution of the outer interface is assimilated to a linear interpolation of AFM roughness measurements acquired before and after experiment. For the “AFM/VSI roughness fit” (light grey squares), the evolution of the outer interface is associated to the mean value between VSI and AFM measurements, their evolution being supposed linear (see text). The sample roughness measured before and after experiment by VSI and AFM is reported in red and green respectively in panel A. Typical fields of view are represented in panels C and D.

Reactivity and physicochemical properties of the fluid/solid interface inferred from XRR and VSI measurements

Traditionally, the mechanisms and rates of mineral dissolution have been indirectly monitored through the evolution of fluid composition [79,80]. In these studies, the non-stoichiometry of elemental release was used to indirectly probe the formation of ASSLs at the fluid-mineral interface[10,28,31]. As mentioned in the introduction, this indirect approach suffers from high uncertainties when it comes to determining the evolution of ASSL thickness and density, particularly at low dissolution rates, principally due to the difficulty of accurately determining the stoichiometry of the small elemental release and, also, of constraining the evolving reacting surface area. Our results show that this challenge can be circumvented, to some extent, by using a combination of XRR and VSI measurements to characterize the rate of ASSL formation at the labradorite-water interface. We were able to detect the formation of ASSLs at the surface of labradorite in all tested conditions, in agreement with previous results on a variety of silicate minerals including feldspars [20]. We also probed independently the reactivity of the outer fluid/layer interface and of the inner layer/mineral interface *in-situ*. This provided an accurate picture of the temporal evolution of the fluid-mineral interface (Figure 7, Figure S3), which enabled unravelling the reaction kinetics. Our results indicate a reaction order with respect to hydrogen ion (corresponding to the power to which the activity of this ion is raised, see eq. 3 and Figure 8) of about 0.77 for the overall dissolution process of labradorite occurring at the inner interface, which is slightly higher than values previously reported for this mineral—typically 0.6—but consistent with the expected range within the feldspar series, typically up to 1.0 for bytownite [80]. Slight differences with previously published data are expected since the protocol used here investigates the reactivity of single cleavage planes, which is known to differ from that of bulk mineral powders [78].

Most of the mean density values of ASSLs estimated from XRR data fall between 1.29 g.cm^{-3} and 1.89 g.cm^{-3}. These measured density values are consistent with the theoretical values for a medium composed of spheres of pure amorphous silica organized within an aqueous medium with either a “dense packing” (face-centered cubic) or a “minimal packing” (estimated from 2D analysis, see “Reactivity and evolution of outer interface” section), corresponding to water-silica mass ratios of 63:10 and 10:14, respectively. They may alternatively be associated with a homogeneous product of hydrated silica. Analysis of samples “XRR3-2.5-80-0-001” and “XRR4-2.5-80-0-010” yielded XRR density estimates exceeding the value reported for bulk anhydrous SiO_2 (2.2 g.cm^{-3}, cf. Iler [81]). Such high values may arise from samples with curved interfaces causing total reflection intensity to be detected at angles exceeding the actual critical angle [9] and are therefore not further discussed. Overall, our results indicate that the ASSL is either hydrated or accommodates significant porosity, which, together with the botryoidal texture of the outer interface, is consistent with the hypothesis that ASSL formation involves significant dissolution-reprecipitation [20,59].

Our experiments show that the dissolution rate of the pristine mineral is impacted by the saturation state of the solution with respect to amorphous silica (Figure 6). From a pure thermodynamic standpoint, only the dissolution rate of the ASSL (and not labradorite) should be impacted by the aqueous silica concentration, because the experiments were conducted at far-from-equilibrium conditions with respect to labradorite. This result indicates that the intrinsic dissolution rate of ASSL significantly modulates the reactivity of labradorite (see section “Passivation by surface layers” below).

The dissolution rate of the ASSL was not directly probed by our XRR measurements, which only probed ASSL thickness. However, the need for frequent z-axis realignment throughout the dissolution experiment to match perfect θ-2θ reflection conditions at the surface of the sample provides additional evidence of the progressive retreat of the outer interface, which was tracked more precisely by VSI on separate samples. Our VSI results indicate that the mean ASSL dissolution rate ranged from 1.07×10^{-7} mol m^{-2} s^{-1} at pH = 1.5 to 1.46×10^{-9} mol m^{-2} s^{-1} at pH = 4 at 80°C in silica-poor solutions. These values are in good agreement with the dissolution rate of amorphous silica observed in other studies. For example, linear extrapolation of our experimental Log(rate)=f(pH) model is consistent (within a factor of 0.5 log unit) with the results of Icenhower and Dove (2000)Icenhower and Dove [82] for dilute solutions at pH = 5.7 at 80°C and also (within the same 0.5 log units factor) with estimates based on Rimstidt and Barnes (2000)Rimstidt and Barnes [83] at a pH comprised between 6.5 and 7.1 at 80°C. In addition, our dissolution rates are consistently 2 to 3 orders of magnitude greater than that of quartz [84], as expected for amorphous SiO_2.

Finally, the observation of surface layer dissolution with a fluid at saturation with respect to amorphous silica supports previous hypothesis suggesting either an enhanced solubility of the ASSL formed on silicates such as wollastonite compared to pure amorphous silica, or that ASSLs dissolve by a different mechanism than amorphous silica [6]. This result however is at odds with observations conducted on ASSLs formed on diopside [85], where the solubility of the ASSLs was suggested to be close to that of α-cristobalite.

In summary, our results suggest that ASSLs formed on labradorite have slightly higher solubility than amorphous SiO_2 but similar dissolution rates. Since the solubility of hydrated amorphous silica would theoretically be decreased compared to pure amorphous silica according to [81], we conclude that the presence in our system of a homogenous layer of hydrated amorphous silica is unlikely. Instead, a layer composed of a rather dense packing of silica-rich spheres surrounded by aqueous solution may form, which would be consistent with a mechanism whereby a botryoidal texture propagates through the layer. Whether the packing, size, or composition of the spheres changes through time still needs to be determined.

As shown in Figure 5, the dissolution rate of ASSL in an acidic solution is also pH-dependent, meaning that hydrogen ions are involved, to some extent, in the dissolution reaction. This feature is generally unexpected for pure amorphous silica [82]. This supports the hypothesis that ASSLs formed on labradorite at $pH > 1.5$ may not consist of pure hydrated SiO_2 [14]. In addition, when the fluid is saturated with respect to amorphous silica (aqueous silica concentrations typically of 5.2×10^{-3} M), the reaction order with respect to hydrogen ion is reduced, showing a reduced impact of the layer on the dissolution rate at more acidic pH values (Figure 8). This is consistent with the formation of different layer-forming phases depending on the pH conditions, the passivating effect of which would be enhanced at conditions closer to neutrality.

The estimate for the activation energy of labradorite dissolution in the present experiments is ~58 kJ mol^{-1}, which is similar to those typically reported for labradorite, at ~42 kJ mol^{-1} [80]. Finally, no difference was detected between the layer growth rate recorded on (001) and (010) faces (Figure 7A). Since no anisotropy of dissolution is expected from amorphous phases such as those constituting the ASSL, we conclude that no compelling evidence of dissolution anisotropy for labradorite could be evidenced here.

Effect of drying on ASSL properties

Our approach, involving a continuously hydrated fluid-mineral interface, is not completely analogous to environmental settings where minerals, glasses, and concrete materials experience drying/wetting cycles. The effect of drying was therefore investigated at three pH conditions (experiments XRR9-1.5-80-SiO2-001, XRR11-2.5-80-SiO2-001, and XRR13-3-80-SiO2-001). As reported in Table S3, drying of ASSLs tends to decrease their apparent density, while having no clear impact on their thickness or roughness. The porosity, defined as the volume proportion of fluid or air in the ASSL, was estimated from SLD values measured *in-situ* or after drying, respectively. The layer was considered to a first approximation as a porous amorphous silica phase, as suggested by its reactivity (cf. previous section). This analysis suggests a drop in the porosity during drying for the experiment conducted under acid conditions (pH=1.5) and an increase of the density at milder pH (pH>1.5) (Table 1). Such behavior cannot be explained by a prospective collapse or dilatation of the porous network during drying since no significant evolution of the thickness of the ASSL could be observed. Alternatively, precipitation of distinct phases from the poral solution, depending on its pH, could explain either the sealing of the porosity by growth and coalescence of the particles forming the layer at pH=1.5 (which can bear higher concentrations of dissolved species), while the precipitation of platelet-like phases could open-up the porosity of layers formed at milder conditions, which are suspected to exhibit higher Al-content [14]. This hypothesis is supported by the larger discrepancy existing between the porosity measured *in-situ* and after drying for the experiment at pH=3 (22.5%) than at pH=2.5 (10.5%). The preliminary results obtained with our approach open interesting avenues for the investigation of dry/wet cycles on ASSL textural properties that still need to be explored in depth.

Measurement	***In-situ***		**dried**	
Experiment	*SLD Layer [10^{-6}.A^{-2}]*	*Porosity %Water (Vol.)*	*SLD Layer [10^{-6}.A^{-2}]*	*Porosity %Air (Vol.)*
XRR9-1.5-80-SiO2-001	14.7	43	14.0	25
XRR11-2.5-80-SiO2-001	15.5	34	10.3	45
XRR13-3-80-SiO2-001	13.2	60	3.4	82

Table 1: Scattering length densities (SLD) and associated estimate of layer's porosity measured *in-situ* or after drying.

Passivation by surface layers

The passivating effect of ASSLs, which results in the reduction of the dissolution rate of primary silicates, has been evidenced in a variety of geological or geochemical contexts [2,9,14,21,61]. In the present study, lower dissolution rates were observed on a reference silicate material (labradorite feldspar) during experiments conducted with silica-rich solutions compared to those that used silica-poor solutions at equivalent pH values. Such contrasting behavior cannot be explained using current analysis approaches, which consist of relating physico-chemical properties of the bulk fluid (e.g. T, pH, and other ion activities) to the overall dissolution rate of the silicate materials (R_{min}), following:

$$R_{min} = \left[\sum_i A_{i,min}.\, exp\left(\frac{-E^i_{a,min}}{RT}\right).\, a_i^{n_{i,min}}\right]\left(1 - exp\left(\frac{s * \Delta Gr}{RT}\right)\right) \qquad (3)$$

where $A_{i,min}$ is an Arrhenius pre-exponential factor; $E^i_{a,min}$, a_i, and $n_{i,min}$ are the activation energy, activity, and reaction order with respect to reactive species i; R is the ideal gas constant; T is absolute temperature; and ΔGr and S are the Gibbs free energy of the dissolution reaction and a dimensionless empirical factor. According to the classical theoretical framework of mineral dissolution kinetics, the affinity term $\left(1 - exp\left(\frac{s*\Delta Gr}{RT}\right)\right)$ equals ~1 in our experiments since the aqueous solutions were at far-from-equilibrium conditions with respect to the dissolution of the primary phase (ΔG_r < -41.8 kJ mol^{-1}, Table S1). Note that this statement holds true even if more sophisticated empirical functions are used, such as the one determined by Taylor, et al. [46] for labradorite. Moreover, in acidic conditions (pH ≤ 4), the only reactive species to be considered is H^+. In short, no effect of the activity of dissolved SiO_2 is anticipated for our system, which is at odds with labradorite dissolution rate in silica-rich solutions being 5 to 50 times lower compared with silica-poor solutions as described above. Therefore, we conclude that the composition of the solution at the inner (labradorite/ASSL) interface must be different from that of the bulk solution, consistent with other recent studies 86. In particular, since temperature was maintained constant, we conclude that the two remaining parameters able to influence the kinetic dissolution rate (namely pH and/or ion concentration) might be significantly higher at the inner interface than in the fluid at least for the silica-rich experiments, and that this discrepancy is higher for experiments conducted in silica-rich fluid than for silica-poor experiments. This hypothesis is supported by the fact that the rate drop observed when saturating the fluid with respect to amorphous silica is more marked for experiments conducted at higher pH, where fluid composition is more sensitive to proton consumption and cation release by the dissolution process. Of note, at pH = 4 with high background concentrations of dissolved silica, pore fluid can only accommodate about 30 ppb of Al^{3+} and Ca^{2+} before reaching the close-to-equilibrium regime domain with respect to labradorite dissolution defined by Taylor, et al. [46]. These conclusions may be related to the overall increase of density observed for most experiments conducted in silica-rich solutions, which may indicate a decrease in the ASSL's porosity and, possibly, transport properties as previously reported for the dissolution of wollastonite [9]. Decreasing density observed for XRR9 and XRR11 experiments suggests however that density may not fully explain transport properties inside ASSLs and that other parameters controlling the spatial organization of the porous network (e.g. tortuosity) may need to be investigated in future using microscopy and surface-sensitive scattering techniques coupled with numerical modeling.

In summary, we hypothesize that the decrease of the dissolution rate of labradorite minerals in silica-rich fluids was due to the passivation by ASSLs formed under these conditions, which decreased the transport properties of reactive species and reaction products through the layer, ultimately leading to higher local pH and/or ion concentration at the inner layer/mineral interface.

On the contrary, for experiments conducted in silica-poor fluids, no clear evidence of passivation and ASSL densification was noted. Two possible explanations can be put forward to explain this observation, in contrast with previous data where passivation could be directly observed [14,21]. First, it is likely that the emergence of passivating properties requires a certain minimal duration for the layer to densify, also called “maturing time” [87]. Analogous time-dependent processes have been previously observed for amorphous phases such as pregibbsite gels [88]. Of note, no clear temporal decrease of the dissolution rate was seen on the timescale of our experiments. Secondly, it is possible that elemental release from accessory phases included in a given primary mineral or assemblage, and especially iron-containing minerals, plays an important role in the buildup of passivating layers. Indeed, formation of a hematite-amorphous silica assemblage, exhibiting passivating properties due to strong Fe(III)-Si chemical interactions [62,89] is one of the few clearly identified mechanism of silicate passivation to date. Contrary to the present study, both in Wild, et al. [14] and Daval, et al. [21] where passivation effect could be observed, the labradorite used contained Fe-bearing mineral inclusions. Such hypothesis, however, would still need to be demonstrated, especially regarding transport of iron from accessory phases to the iron-free silicate surface.

Existing dissolution rate laws are based almost exclusively on laboratory experiments consisting in immersing mineral grains in reactive fluids at high temperature and low pH conditions and recording dissolution through elemental release into solution. The methodology developed here provides complementary data that can help shed light on silicate dissolution in natural settings. In particular, we were able to precisely quantify two properties critical to extrapolating laboratory results to natural settings and larger time and spatial scales: the rates of dissolution of the pristine mineral and of the ASSL and their associated activation energies. In addition, we provided indirect evidence for changes in the pore fluid chemistry of the ASSL, possibly related to the apparent transport properties of this phase. With regards to implications for silicate weathering in field conditions, our results suggest that circum-neutral pH values, silica-rich fluids, the presence of complex mineralogical assemblages including Fe-rich phases, long time scales, and drying-wetting cycles all tend to favor the formation of ASSLs with reduced porosity and transport properties. The methodology developed here should therefore enable to better characterize the physicochemical evolution of the silica-rich surface layers on a wide range of silicate materials, enabling to relate the dissolution rates of silicate materials observed at the macroscale to the transport properties of nanoporous silica-rich layers, which have been extensively studied both from theoretical and experimental perspectives [57,67-71].

CONCLUSIONS

The present study tested a novel methodology to probe *in-situ* the formation and properties of amorphous silica-rich surface layers (ASSLs) developed at a fluid-silicate interface.

Our approach enabled precise quantification of the formation of ASSLs on labradorite feldspar, a silicate mineral representative of the continental crust. We quantified ASSL density, thickness, and roughness by X-ray reflectivity while independently probing ASSL reactivity by vertical scanning interferometry. Our results suggest that the ASSLs have a significant effect on the dissolution rate of the primary mineral: our experiments revealed a drop in the dissolution rate of labradorite in silica-rich solutions compared to silica-poor solutions, where both conditions were far-from equilibrium with respect to the dissolution of this primary phase in the bulk fluid. Our results suggest that ASSLs formed in silica-rich fluids have distinct transport properties resulting in either higher ion activities, higher pH, or both in the pore solution controlling the dissolution of the primary phase.

Overall, our findings underline the need for an improved understanding of the processes controlling local physico-chemical parameters at the interface with the dissolving silicate, which may differ from those recorded in bulk fluid. The methodology developed here is a valuable tool for investigating silicate dissolution. In addition to complementary from bulk fluid analysis, it has the potential to enable the determination of the relevant parameters (e.g. local fluid pH and saturation conditions actually driving the dissolution process at the inner layer-silicate interface) for onsite applications and important industrial processes.

AUTHOR INFORMATION

Corresponding Author

* Andlinger Center for Energy and the Environment, Princeton University, Princeton, NJ 08544, USA; e-mail: bwild@princeton.edu

Author Contributions

The manuscript was written through contributions of all authors. All authors have given approval to the final version of the manuscript.

ACKNOWLEDGMENT

A. Aubert and V. Magnin are acknowledged for their technical support during synchrotron measurement campaigns. A. Putnis, J. Hövelmann, K. Czaja and the Mineralogical & Geological Museum of Harvard University are warmly acknowledged for providing labradorite samples (Ref. MGMH#135998). This project was funded by the VALVE project (EC2CO-BIOHEFECT program coordinated by the CNRS-INSU) attributed to D. Daval. B. Wild was supported by Princeton University's Andlinger Center for Energy and Environment through its Distinguished Postdoctoral Fellows program. The relevance of this study and the quality of the manuscript was significantly improved by insightful comments from Thorsten Geisler-Wierwille, Moritz Fritzsche and two anonymous reviewers.

ABBREVIATIONS

ASSLs, amorphous silica-rich surface layers; VSI, vertical scanning interferometry; XRR, X-ray reflectivity;

TST, transition state theory; BET, Brunauer-Emmett-Teller; AFM, atomic force microscopy; EBSD, electron backscatter diffraction; SEM, scanning electron microscope; PTFE, polytetrafluoroethylene; RTV, room-temperature-vulcanizing; ESRF, European synchrotron radiation facility; SLD, scattering length density; Ab, Albite ($NaAlSi_3O_8$); An, Anorthite ($CaAl_2Si_2O_8$); Or, Orthoclase ($KAlSi_3O_8$).

SUPPORTING INFORMATION AVAILABLE

Summary of experiments conducted in this study, tables of best fit parameters associated to reflectivity data, Table of surface retreat measured by VSI, example of treatment of reflectivity data, AFM topography of a reacted portion of labradorite.

REFERENCES

1 Bearat, H., McKelvy, M. J., Chizmeshya, A. V. G., Gormley, D., Nunez, R., Carpenter, R. W., Squires, K. & Wolf, G. H. Carbon sequestration via aqueous olivine mineral carbonation: Role of passivating layer formation. Environ. Sci. Technol. 40, 4802-4808 (2006).

2 Daval, D., Sissmann, O., Menguy, N., Saldi, G. D., Guyot, F., Martinez, I., Corvisier, J., Garcia, B., Machouk, I., Knauss, K. G. et al. Influence of amorphous silica layer formation on the dissolution rate of olivine at 90°C and elevated pCO(2). Chem. Geol. 284, 193-209 (2011).

3 Johnson, N. C., Thomas, B., Maher, K., Rosenbauer, R. J., Bird, D. & Brown Jr, G. E. Olivine dissolution and carbonation under conditions relevant for in situ carbon storage. Chem. Geol. 373, 93-105 (2014).

4 Maher, K., Johnson, N. C., Jackson, A., Lammers, L. N., Torchinsky, A. B., Weaver, K. L., Bird, D. K. & Brown Jr, G. E. A spatially resolved surface kinetic model for forsterite dissolution. Geochim. Cosmochim. Acta 174, 313-334 (2016).

5 Daval, D., Martinez, I., Corvisier, J., Findling, N., Goffe, B. & Guyot, F. Carbonation of Ca-bearing silicates, the case of wollastonite: Experimental investigations and kinetic modeling. Chem. Geol. 265, 63-78 (2009).

6 Weissbart, E. J. & Rimstidt, D. J. Wollastonite: Incongruent dissolution and leached layer formation. Geochim. Cosmochim. Acta 64, 4007-4016 (2000).

7 Ruiz-Agudo, E., Putnis, C. V., Rodriguez-Navarro, C. & Putnis, A. Mechanism of leached layer formation during chemical weathering of silicate minerals. Geology 40, 947-950 (2012).

8 Schott, J., Pokrovsky, O. S., Spalla, O., Devreux, F., Gloter, A. & Mielczarski, J. A. Formation, growth and transformation of leached layers during silicate minerals dissolution: The example of wollastonite. Geochim. Cosmochim. Acta 98, 259-281 (2012).

9 Daval, D., Bernard, S., Rémusat, L., Wild, B., Guyot, F., Micha, J. S., Rieutord, F., Magnin, V. & Fernandez-Martinez, A. Dynamics of altered surface layer formation on dissolving silicates. Geochim. Cosmochim. Acta 209, 51-69 (2017).

10 Lagache, M. New data on the kinetics of the dissolution of alkali feldspars at 200°C in CO2 charged water. Geochim. Cosmochim. Acta 40, 157-161 (1976).

11 Casey, W. H., Westrich, H. R., Massis, T., Banfield, J. F. & Arnold, G. W. The surface of labradorite feldspar after acid hydrolysis. Chem. Geol. 78, 205-218 (1989).

12 Casey, W. H., Westrich, H. R., Banfield, J. F., Ferruzzi, G. & Arnold, G. W. Leaching and reconstruction at the surface of dissolving chain-silicate minerals. Nature 366, 253-256 (1993).

13 Hellmann, R., Penisson, J.-M., Hervig, R. L., Thomassin, J.-H. & Abrioux, M.-F. An EFTEM/HRTEM high-resolution study of the near surface of labradorite feldspar altered at acid pH: evidence for interfacial dissolution-reprecipitation. Physics and Chemistry of Minerals 30, 192-197 (2003).

14 Wild, B., Daval, D., Guyot, F., Knauss, K. G., Pollet-Villard, M. & Imfeld, G. pH-dependent control of feldspar dissolution rate by altered surface layers. Chem. Geol. 442, 148-159 (2016).

15 Cailleteau, C., Angeli, F., Devreux, F., Gin, S., Jestin, J., Jollivet, P. & Spalla, O. Insight into silicate-glass corrosion mechanisms. Nature Materials 7, 978-983 (2008).

16 Verney-Carron, A., Gin, S., Frugier, P. & Libourel, G. Long-term modeling of alteration-transport coupling: Application to a fractured Roman glass. Geochim. Cosmochim. Acta 74, 2291-2315 (2010).

17 Geisler, T., Nagel, T., Kilburn, M. R., Janssen, A., Icenhower, J. P., Fonseca, R. O. C., Grange, M. & Nemchin, A. A. The mechanism of borosilicate glass corrosion revisited. Geochim. Cosmochim. Acta 158, 112-129 (2015).

18 Gin, S., Jollivet, P., Fournier, M., Angeli, F., Frugier, P. & Charpentier, T. Origin and consequences of silicate glass passivation by surface layers. Nat. Commun. 6, 6360 (2015).

19 Nugent, M. A., Brantley, S. L., Pantano, C. G. & Maurice, P. A. The influence of natural mineral coatings on feldspar weathering. Nature 395, 588-591 (1998).

20 Hellmann, R., Wirth, R., Daval, D., Barnes, J.-P., Penisson, J.-M., Tisserand, D., Epicier, T., Florin, B. & Hervig, R. L. Unifying natural and laboratory chemical weathering with interfacial dissolution–reprecipitation: A study based on the nanometer-scale chemistry of fluid–silicate interfaces. Chem. Geol. 294–295, 203-216 (2012).

21 Daval, D., Calvaruso, C., Guyot, F. & Turpault, M.-P. Time-dependent feldspar dissolution rates resulting from surface passivation: Experimental evidence and geochemical implications. Earth and Planetary Science Letters 498, 226-236 (2018).

22 Monteiro, P. J. M., Miller, S. A. & Horvath, A. Towards sustainable concrete. Nature Materials 16, **698** (2017).

23 Gin, S., Collin, M., Jollivet, P., Fournier, M., Minet, Y., Dupuy, L., Mahadevan, T., Kerisit, S. & Du, J. Dynamics of self-reorganization explains passivation of silicate glasses. Nat. Commun. 9, 2169 (2018).

24 Park, A.-H. A. & Fan, L.-S. CO2 mineral sequestration: physically activated dissolution of serpentine and pH swing process. Chemical Engineering Science 59, 5241-5247 (2004).

25 Noiriel, C. & Daval, D. Pore-scale geochemical reactivity associated with CO2 storage: new frontiers at the fluid–solid interface. Accounts of Chemical Research 50, 759-768 (2017).

26 Correns, C. W. & von Engelhardt, W. Neue Untersuchungen über die Verwitterung des Kalifeldspates. Naturwissenschaften 26, 137-138 (1938).

27 Luce, R. W., Bartlett, R. W. & Parks, G. A. Dissolution kinetics of magnesium silicates. Geochim. Cosmochim. Acta 36, 33-50 (1972).

28 Paces, T. Chemical characteristics and equilibration in natural water-felsic rock-CO2 system. Geochim. Cosmochim. Acta 36, 217-240 (1972).

29 Muir, I. J., Michael Bancroft, G. & Wayne Nesbitt, H. Characteristics of altered labradorite surfaces by SIMS and XPS. Geochim. Cosmochim. Acta 53, 1235-1241 (1989).

30 Petit, J.-C., Dran, J.-C., Schott, J. & Mea, G. D. New evidence on the dissolution mechanism of crystalline silicates by MeV ion beam techniques. Chem. Geol. 76, 365-369 (1989).

31 Hellmann, R., Eggleston, C. M., Hochella, M. F. J. & Crerar, D. A. The formation of leached layers on albite surfaces during dissolution under hydrothermal conditions. Geochim. Cosmochim. Acta 54, 1267-1281 (1990).

32 Inskeep, W. P., Nater, E. A., Bloom, P. R., Vandervoort, D. S. & Erich, M. S. Characterization of laboratory weathered labradorite surfaces using X-ray photoelectron

spectroscopy and transmission electron microscopy. Geochim. Cosmochim. Acta 55, 787-800 (1991).

33 Muir, I. J. & Nesbitt, H. W. Effects of aqueous cations on the dissolution of labradorite feldspar. Geochim. Cosmochim. Acta 55, 3181-3189 (1991).

34 Shotyk, W. & Nesbitt, H. W. Incongruent and congruent dissolution of plagioclase feldspar - effect of feldspar compositionand ligand complexation. Geoderma 55, 55-78 (1992).

35 Shotyk, W. & Metson, J. B. Secondary ion mass spectrometry (SIMS) and its application to chemical weathering. Reviews of Geophysics 32, 197-220 (1994).

36 Schweda, P., Sjoberg, L. & Sodervall, U. Near-surface composition of acid-leached labradorite investigated by SIMS. Geochim. Cosmochim. Acta 61, 1985-1994 (1997).

37 Chen, Y. & Brantley, S. L. Dissolution of forsteritic olivine at 65°C and $2<pH<5$. Chem. Geol. 165, 267-281 (2000).

38 Nesbitt, H. W. & Skinner, W. M. Early development of Al, Ca, and Na compositional gradients in labradorite leached in pH 2 HCl solutions. Geochim. Cosmochim. Acta 65, 715-727 (2001).

39 Putnis, C. V., Tsukamoto, K. & Nishimura, Y. Direct observations of pseudomorphism: compositional and textural evolution at a fluid-solid interface. Am. Miner. 90, 1909-1912 (2005).

40 Jordan, G., Higgins, S. R., Eggleston, C. M., Swapp, S. M., Janney, D. E. & Knauss, K. G. Acidic dissolution of plagioclase: in-situ observations by hydrothermal atomic force microscopy. Geochim. Cosmochim. Acta 63, 3183-3191 (1999).

41 Aagaard, P. & Helgeson, H. C. Thermodynamic and kinetic constraints on reaction-rates among minerals and aqueous solutions. 1. Theoretical considerations. American Journal of Science 282, 237-285 (1982).

42 Berner, R. A. & Holdren, G. R. Mechanism of feldspar weathering - some observational evidence. Geology 5, 369-372 (1977).

43 Berner, R. A. & Holdren, G. R. Mechanism of feldspar weathering .2. Observations of feldspars from soils. Geochim. Cosmochim. Acta 43, 1173-1186 (1979).

44 Holdren, G. R. & Berner, R. A. Merchanism of feldspar weathering. 1. Experimental studies. Geochim. Cosmochim. Acta 43, 1161-1171 (1979).

45 Oelkers, E. H., Schott, J. & Devidal, J.-L. The effect of aluminum, pH, and chemical affinity on the rates of aluminosilicate dissolution reactions. Geochim. Cosmochim. Acta 58, 2011-2024 (1994).

46 Taylor, A. S., Blum, J. D. & Lasaga, A. C. The dependence of labradorite dissolution and Sr isotope release rates on solution saturation state. Geochim. Cosmochim. Acta 64, 2389-2400 (2000).

47 Nagy, K. L., Blum, A. E. & Lasaga, A. C. Dissolution and precipitation kinetics of kaolinite at 80 degrees C and pH 3; the dependence on solution saturation state. American Journal of Science 291, 649-686 (1991).

48 Lasaga, A. C. in Chemical weathering rates of silicate minerals Vol. 31 (eds Art F. White & Susan L. Brantley) 23-86 (1995).

49 Grambow, B. & Muller, R. First-order dissolution rate law and the role of surface layers in glass performance assessment. J. Nucl. Mater. 298, 112-124 (2001).

50 Bourcier, W. L., Peiffer, D. W., Knauss, K. G., McKeegan, K. D. & Smith, D. K. A Kinetic model for B\borosilicate glass dissolution based on the dissolution affinity of a surface alteration layer. MRS Online Proceedings Library Archive 176, 1-10 (1989).

51 Oelkers, E. H. & Schott, J. Experimental study of anorthite dissolution and the relative mechanism of feldspar hydrolysis. Geochim. Cosmochim. Acta 59, 5039-5053 (1995).

52 Daux, V., Guy, C., Advocat, T., Crovisier, J. L. & Stille, P. Kinetic aspects of basaltic glass dissolution at 90°C: role of aqueous silicon and aluminium. Chem. Geol. 142, 109-126 (1997).

53 Oelkers, E. H. General kinetic description of multioxide silicate mineral and glass dissolution. Geochim. Cosmochim. Acta 65, 3703-3719 (2001).

54 Lüttge, A. Crystal dissolution kinetics and Gibbs free energy. Journal of Electron Spectroscopy and Related Phenomena 150, 248-259 (2006).

55 Devreux, F., Ledieu, A., Barboux, P. & Minet, Y. Leaching of borosilicate glasses. II. Model and Monte-Carlo simulations. J. Non-Cryst. Solids 343, 13-25 (2004).

56 Rebiscoul, D., Van der Lee, A., Rieutord, F., Ne, F., Spalla, O., El-Mansouri, A., Frugier, P., Ayral, A. & Gin, S. Morphological evolution of alteration layers formed during nuclear glass alteration: new evidence of a gel as a diffusive barrier. J. Nucl. Mater. 326, 9-18 (2004).

57 Gin, S. p., Guittonneau, C., Godon, N., Neff, D., Rebiscoul, D., Cabié, M. & Mostefaoui, S. Nuclear glass durability: new insight into alteration layer properties. The Journal of Physical Chemistry C 115, 18696-18706 (2011).

58 Gin, S., Neill, L., Fournier, M., Frugier, P., Ducasse, T., Tribet, M., Abdelouas, A., Parruzot, B., Neeway, J. & Wall, N. The controversial role of inter-diffusion in glass alteration. Chem. Geol. 440, 115-123 (2016).

59 Ruiz-Agudo, E., King, H. E., Patiño-López, L. D., Putnis, C. V., Geisler, T., Rodriguez-Navarro, C. & Putnis, A. Control of silicate weathering by interface-coupled dissolution-precipitation processes at the mineral-solution interface. Geology 44, 567-570 (2016).

60 Sissmann, O., Daval, D., Brunet, F., Guyot, F., Verlaguet, A., Pinquier, Y., Findling, N. & Martinez, I. The deleterious effect of secondary phases on olivine carbonation yield: Insight from time-resolved aqueous-fluid sampling and FIB-TEM characterization. Chem. Geol. 357, 186-202 (2013).

61 Saldi, G. D., Daval, D., Morvan, G. & Knauss, K. G. The role of Fe and redox conditions in olivine carbonation rates: an experimental study of the rate limiting reactions at 90 and 150 °C in open and closed systems. Geochim. Cosmochim. Acta 118, 157-183 (2013).

62 Saldi, G. D., Daval, D., Guo, H., Guyot, F., Bernard, S., Le Guillou, C., Davis, J. A. & Knauss, K. G. Mineralogical evolution of Fe–Si-rich layers at the olivine-water interface during carbonation reactions. Am. Miner. 100, 2655-2669 (2015).

63 Hellmann, R., Cotte, S., Cadel, E., Malladi, S., Karlsson, L. S., Lozano-Perez, S., Cabié, M. & Seyeux, A. Nanometre-scale evidence for interfacial dissolution–reprecipitation control of silicate glass corrosion. Nat Mater 14, 307-311 (2015).

64 Casey, W. H. Glass and mineral corrosion dynamics and durability. Nature Materials 7, 930-932 (2008).

65 White, A. F. & Brantley, S. L. The effect of time on the weathering of silicate minerals: why do weathering rates differ in the laboratory and field? Chem. Geol. 202, 479-506 (2003).

66 Fischer, C., Arvidson, R. S. & Lüttge, A. How predictable are dissolution rates of crystalline material? Geochim. Cosmochim. Acta 98, 177-185 (2012).

67 Cailleteau, C., Devreux, F., Spalla, O., Angeli, F. & Gin, S. Why do certain glasses with a high dissolution rate undergo a low degree of corrosion? The Journal of Physical Chemistry C 115, 5846-5855 (2011).

68 Bourg, I. C. & Steefel, C. I. Molecular dynamics simulations of water structure and diffusion in silica nanopores. The Journal of Physical Chemistry C 116, 11556-11564 (2012).

69 Rébiscoul, D., Cambedouzou, J., Matar Briman, I., Cabié, M., Brau, H. P. & Diat, O. Water dynamics in nanoporous alteration layer coming from glass alteration: an experimental approach. The Journal of Physical Chemistry C 119, 15982-15993 (2015).

70 Neeway, J. J., Kerisit, S. N., Liu, J., Zhang, J., Zhu, Z., Riley, B. J. & Ryan, J. V. Ion-exchange interdiffusion model with potential application to long-term nuclear waste glass performance. The Journal of Physical Chemistry C 120, 9374-9384 (2016).

71 Collin, M., Gin, S., Dazas, B., Mahadevan, T., Du, J. & Bourg, I. C. Molecular dynamics simulations of water structure and diffusion in a 1 nm diameter silica nanopore as a function of surface charge and alkali metal counterion identity. The Journal of Physical Chemistry C 122, 17764-17776 (2018).

72 Hövelmann, J., Austrheim, H. & Putnis, A. Cordierite formation during the experimental reaction of plagioclase with Mg-rich aqueous solutions. Contributions to Mineralogy and Petrology 168, 1063 (2014).

73 Arvidson, R. S., Beig, M. S. & Lüttge, A. Single-crystal plagioclase feldspar dissolution rates measured by vertical scanning interferometry. Am. Miner. 89, 51-56 (2004).

74 Nečas, D. & Klapetek, P. Gwyddion: an open-source software for SPM data analysis. Central European Journal of Physics 10, 181-188 (2012).

75 Nelson, A. Co-refinement of multiple-contrast neutron/X-ray reflectivity data using MOTOFIT. Journal of Applied Crystallography 39, 273-276 (2006).

76 Bowen, D. K., Tanner, B. K., Wormington, M., Panaccione, C., Matney Kevin, M. & Bowen, D. K. Characterization of structures from X-ray scattering data using genetic algorithms.

Philosophical Transactions of the Royal Society of London. Series A: Mathematical, Physical and Engineering Sciences 357, 2827-2848 (1999).

77 Marquardt, D. An Algorithm for least-squares estimation of nonlinear parameters. Journal of the Society for Industrial and Applied Mathematics 11, 431-441 (1963).

78 Pollet-Villard, M., Daval, D., Ackerer, P., Saldi, G. D., Wild, B., Knauss, K. G. & Fritz, B. Does crystallographic anisotropy prevent the conventional treatment of aqueous mineral reactivity? A case study based on K-feldspar dissolution kinetics. Geochim. Cosmochim. Acta 190, 294-308 (2016).

79 Schott, J., Pokrovsky, O. S. & Oelkers, E. H. The link between mineral dissolution/precipitation kinetics and solution chemistry. Thermodynamics and Kinetics of Water-Rock Interaction 70, 207-258 (2009).

80 Palandri, J. L. & Kharaka, Y. K. A compilation of rate parameters of water-mineral interaction kinetics for application to geochemical modeling. 70 (U.S. Geological Survey, Open File Report, 2004).

81 Iler, R. K. The chemistry of silica : solubility, polymerization, colloid and surface properties, and biochemistry / Ralph K. Iler. (Wiley, 1979).

82 Icenhower, J. P. & Dove, P. M. The dissolution kinetics of amorphous silica into sodium chloride solutions: effects of temperature and ionic strength. Geochim. Cosmochim. Acta 64, 4193-4203 (2000).

83 Rimstidt, J. D. & Barnes, H. L. The kinetics of silica-water reactions. Geochim. Cosmochim. Acta 44, 1683-1699 (1980).

84 Tester, J. W., Worley, W. G., Robinson, B. A., Grigsby, C. O. & Feerer, J. L. Correlating quartz dissolution kinetics in pure water from 25 to 625°C. Geochim. Cosmochim. Acta 58, 2407-2420 (1994).

85 Daval, D., Hellmann, R., Saldi, G. D., Wirth, R. & Knauss, K. G. Linking nm-scale measurements of the anisotropy of silicate surface reactivity to macroscopic dissolution rate laws: New insights based on diopside. Geochim. Cosmochim. Acta 107, 121-134, (2013).

86 Geisler, T., Dohmen, L., Lenting, C. & Fritzsche, M. B. K. Real-time in situ observations of reaction and transport phenomena during silicate glass corrosion by fluid-cell Raman spectroscopy. Nature Materials (2019).

87 Bottero, J. Y., Cases, J. M., Fiessinger, F. & Poirier, J. E. Studies of hydrolyzed aluminium-chloride solutions. 1.Nature of aluminium species and composition of aqueous solutions. J. Phys. Chem. 84, 2933-2939 (1980).

88 McHardy, W. J. & Thomson, A. P. Conditions for the formation of bayerite and gibbsite. Mineralogical magazine 38, 358-368 (1971).

89 Schott, J. & Berner, R. A. X-Ray Photoelectron studies of the mechanism of iron silicate dissolution during weathering. Geochim. Cosmochim. Acta 47, 2233-2240 (1983).